Available online at www.sciencedirect.com
SCIENCE DIRECT®
ELSEVIER
Journal of Magnetism and Magnetic Materials 260 (2003) 319–329
Journal of magnetism and magnetic materials
www.elsevier.com/locate/jmmm

# Ion beam synthesis of magnetic Co–Pt alloys in $Al_2O_3$

S.P. Withrow[a,*], C.W. White[a], J.D. Budai[a], L.A. Boatner[a], K.D. Sorge[a], J.R. Thompson[a,b], R. Kalyanaraman[c]

[a] *Oak Ridge National Laboratory, P.O. Box 2008, Oak Ridge, TN 37831, USA*
[b] *University of Tennessee, Knoxville, TN, USA*
[c] *Washington University, St. Louis, MI, USA*

Received 29 April 2002; received in revised form 27 August 2002

**Abstract**

Ion implantation followed by thermal processing has been used to synthesize nanoparticles of cobalt–platinum (Co–Pt) alloys in single-crystal $Al_2O_3$. Several phases, including CoPt in the $L1_0$ structure, $Co_3Pt$, and $CoPt_3$ that has the $L1_2$ structure, are selectively formed by varying the atomic ratio of implanted Co and Pt. These alloys are crystallographically oriented with respect to the host $Al_2O_3$ matrix, exhibiting multiple distinct orientations. Rutherford backscattering and X-ray diffraction have been used to study the influence of the processing conditions, including temperature and dose, on the formation of the alloys. The degree of chemical ordering in the $L1_0$ and $L1_2$ phases is not high and it is not improved significantly with long annealing times. Magnetization studies have been conducted using a SQUID magnetometer. Coercivities as high as 14.2 kOe (9.7 kOe) at 5 K with the field normal (parallel) to the surface have been measured, and they remain significant at room temperature and above. The coercivity is a function of the Pt fraction in the alloy.
© 2002 Elsevier Science B.V. All rights reserved.

*PACS:* 75.50.Kj; 75.50.Vv; 41.75.Ak

*Keywords:* Ion implantation synthesis; Co–Pt alloys; CoPt; $Co_3Pt$; $CoPt_3$; Nanocrystalline magnetic materials

## 1. Introduction

Cobalt–platinum (Co–Pt) intermetallic alloy films and nanoparticles can be synthesized over a wide range of compositions. For near-equiatomic stoichiometries, a face centered cubic (FCC) CoPt disordered phase as well as an ordered face centered tetragonal (FCT) phase have been reported [1–5]. Both of these phases are ferromagnetic and magnetically hard [6]. FCT CoPt has the $L1_0$ structure with alternating (0 0 1) planes of Co atoms and Pt atoms resulting in uniaxial magnetocrystalline anisotropy along the (0 0 1) axis. A CoPt alloy with mixed phases and only partially ordered into the FCT structure can still exhibit a large magnetic anisotropy [7]. For either Co- or Pt-rich alloys where the composition ratio is close to 75:25, either a chemically disordered or an ordered phase can be formed. Disordered $CoPt_3$ [8] or $Co_3Pt$ [9,10] is FCC. Ordered $CoPt_3$ [8,11] has the

*Corresponding author. Tel.: +865-576-6719; fax: +865-576-6720.
*E-mail address:* withrowsp@ornl.gov (S.P. Withrow).

0304-8853/03/$ - see front matter © 2002 Elsevier Science B.V. All rights reserved.
PII: S0304-8853(02)01322-7

cubic $L1_2$ structure. Although the ordered $L1_2$ phase has been theoretically predicted for a $Co_3Pt$ stoichiometry, [12] it has not been experimentally reported. However, an ordered HCP $Co_3Pt$ phase has been prepared by several groups [9,13,14]. Alloys at these compositions can also exhibit interesting ferromagnetic behavior [15].

Various techniques have been used to prepare Co–Pt films and particles, including sputtering [1,2,5,7,8], e-beam evaporation [16], molecular beam epitaxy [9] and microemulsion deposition [4]. In this work, sequential ion implantation of overlapping Co and Pt distributions followed by thermal treatment has been used to synthesize ordered Co–Pt alloys in the near-surface region of single-crystal $Al_2O_3$ substrates. The alloys thus formed can be crystallographically oriented with respect to the crystalline matrix, and they exhibit significant magnetic behavior as detailed below. Transmission electron microscopy (TEM) confirms that under these processing conditions nanoparticles are formed over the range of compositions, similar to the microstructure seen for Fe–Pt alloys synthesized using similar processing [17,18].

Ion implantation has become a useful technique for synthesizing nanometer-sized particles with interesting and unique properties in the near-surface of a variety of host matrices [19]. To our knowledge, this is the first reported formation of Co–Pt alloys using implantation methods, although ion beams have been used to irradiate and partially mix deposited films of alternating Co and Pt layers [7,20] and Pt implantation has been used to modify pre-existing Co nanoparticles in sapphire [21,22]. Co–Pt phases exist over a range of alloy compositions. For example, it has been reported that the ordered FCT phase forms in alloys of $Co_{1-x}Pt_x$ where $\sim 40 < x < \sim 70$, [2] with the degree of ordering and magnetic properties expected to be dependent on composition. Hence, controlling the composition offers interesting possibilities for tailoring the alloy properties. Ion implantation is therefore an ideal technique to use for the synthesis of Co–Pt particles since the formation of alloy phases with different compositions is conveniently achieved by varying the Co-to-Pt implantation ratio.

## 2. Experimental procedure

Disks of single-crystal, *c*-axis-oriented $\alpha$-$Al_2O_3$ were used as host substrates. Cobalt ions at 325–360 keV and platinum ions at 910 keV were sequentially implanted, with the implant energies chosen to give overlapping concentration profiles with a projected range of $\sim 150$ nm [23]. Implant doses of $0.5–1 \times 10^{17}/cm^2$ were used for Co, and the Pt doses were chosen to give the desired Pt atomic fraction $x$ in the alloy where $x = \text{Pt dose}/(\text{Co} + \text{Pt doses})$. Samples were prepared with $x$ in the range 26–73%. Reference in this work to specific $Co_{1-x}Pt_x$ alloys indicates the alloy ratio as experimentally measured by Rutherford backscattering (RBS). The $Al_2O_3$ substrates were implanted either at 550°C for the Co and 500°C for the Pt (high-temperature implant conditions) or at 200°C for both species. The elevated temperatures were used in order to reduce implantation damage in the $Al_2O_3$ matrix. The implanted samples were annealed in a quartz tube furnace in a flowing ambient of Ar + 4% $H_2$ gas for up to 2 h at 1100°C and then cooled slowly to room temperature. Some samples were annealed for longer times at lower temperatures with or without a prior 1100°C anneal. RBS-ion channeling (2.3 MeV $He^{2+}$) and X-ray diffraction (Cu K$\alpha$ radiation in both powder and four-circle diffractometers) were used to characterize the samples. Plan-view TEM micrographs show that nanoparticles are formed over the full range of compositions studied here. The static magnetic response of the synthesized materials was investigated using a SQUID magnetometer with the samples held at temperatures between 5 and 400 K in applied fields up to $\pm 65$ kOe ($\pm 6.5$ T). The diamagnetic background of the $Al_2O_3$ host was subtracted from the measured SQUID results.

## 3. Results and discussion

X-ray diffraction results from $Co_{1-x}Pt_x$ in $Al_2O_3$ for three selected compositions $x$ are given in Fig. 1. These spectra are from annealed samples prepared with Co:Pt implantation ratios chosen close to $Co_3Pt$, CoPt, and $CoPt_3$ stoichiometries.

For all three spectra, the Co ions were implanted at 550°C and the Pt at 500°C. The host matrix was not completely amorphized by any of these implants, as determined from RBS spectra. All samples were annealed for 2 h at 1100°C. Additional annealing at 700°C for 17 and 120 h was made for the samples used to obtain the spectra in Figs. 1a and c, respectively. The $\Theta - 2\Theta$ scans were made along the $c$-axis (normal axis) of the $Al_2O_3$ substrate. As expected, a strong (0 0 0 6) reflection from the $\alpha$-$Al_2O_3$ matrix at $2\Theta = 41.68°$ is present in all three graphs. The additional lines present in the spectra arise from the $Co_{1-x}Pt_x$ nanoparticles that form during the sample anneal.

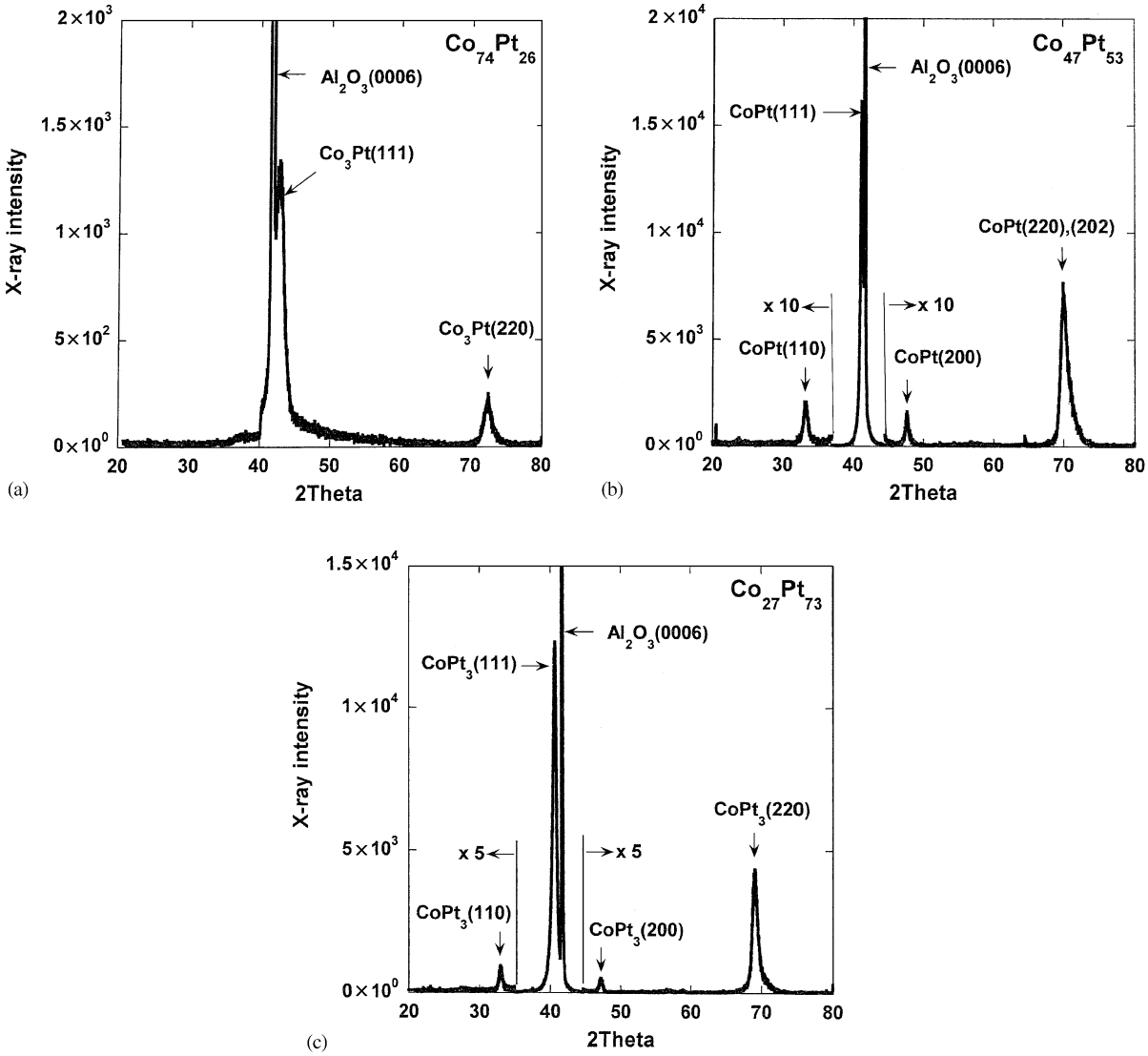


Fig. 1. X-ray diffraction $\Theta - 2\Theta$ scans along the (0 0 0 6) axis of the $Al_2O_3$ substrate after implantation of three different ratios of Co and Pt followed by thermal annealing. Implantation was at 550°C (Co) and 500°C (Pt) for all three samples. (a) $Co_{74}Pt_{26}$ annealed at 1100°C for 2 h in Ar + 4%$H_2$ then at 700°C for 17 h in Ar + 4%$H_2$, (b) $Co_{47}Pt_{53}$ annealed at 1100°C for 2 h in Ar + 4%$H_2$, and (c) $Co_{27}Pt_{73}$ annealed at 1100°C for 2 h in Ar + 4%$H_2$ then at 700°C for 120 h in Ar + 4%$H_2$.

Without the anneal, no lines from Co–Pt are seen. X-ray rocking curves indicate that the alloys are oriented with respect to the $Al_2O_3$ lattice.

The atomic structure of the Co–Pt alloy formed depends on the implantation ratio. For the Co-rich implant conditions of Fig. 1a ($Co_{74}Pt_{26}$), reflections from $Co_3Pt$ are observed. The most intense scattering is in the (1 1 1) reflection at $2\Theta = 42.6°$. Weaker intensity is seen from the (2 2 0) orientation at 72.8°. The binary alloy phase diagram for Co–Pt [24] does not show a stoichiometric alloy for this composition although more recently several authors have reported both a disordered FCC [10] and a chemically ordered HCP [9,13,14] phase. The $Co_3Pt$ lattice constant calculated from the $2\Theta$ angle of both the (1 1 1) and (2 2 0) reflections is $a = 3.67$ Å, which is in agreement with that reported by Ferrer for disordered FCC $Co_3Pt$ [10]. For a sample implanted to the same concentration but with the substrate held at 200°C, very weak scattering is seen at $2\Theta = 34.8°$, which is forbidden for a disordered FCC alloy. This may be an indication of some small amount of chemical ordering in the $Co_3Pt$ phase for samples prepared using the lower implantation temperatures.

X-ray results are shown in Fig. 1b for a slightly Pt-rich implant, $Co_{47}Pt_{53}$. Diffraction lines from several CoPt reflections are observed. The strongest line is the CoPt(1 1 1), with additional but weaker lines from (1 1 0), (2 0 0), and unresolved (2 2 0) and (2 0 2) reflections. These multiple peaks indicate that several orientations of the alloy with respect to the (0 0 0 6) axis (normal to the sample surface) of the matrix are present. X-ray powder diffraction calculations predict the theoretical intensity of the (2 2 0) reflection to be 19% of the (1 1 1) peak. Hence, while a majority of the CoPt alloy observed in this spectrum is oriented with the (1 1 1) axis along the substrate (0 0 0 6) axis, a significant minority of the alloy has its (1 1 0) axis along the substrate (0 0 0 6) axis. High-resolution X-ray results obtained from a $Co_{49}Pt_{51}$ sample showed that particles with both of these normal orientations to be aligned in-plane with the substrate as well. For the nanoparticles oriented with (1 1 1) perpendicular, the in-plane orientation was found to be CoPt[$1\,\bar{1}\,1$] parallel to $Al_2O_3$[$1\,0\,\bar{1}\,0$] with a 60° rotation. For (1 1 0) perpendicular particles, the in-plane orientation was CoPt[$1\,\bar{1}\,0$] parallel to $Al_2O_3$[$1\,0\,\bar{1}\,0$] with a 60° rotation. The (1 1 0) reflection in Fig. 1b is a superstructure reflection and indicates that at least some of the CoPt has the compositionally ordered FCT $L1_0$ microstructure. This reflection is forbidden for a disordered FCC CoPt phase. From the $2\Theta$ angle of the (1 1 1) peak in Fig. 1b, the calculated (1 1 1) layer spacing is 2.19 Å. This is slightly greater ($\sim$1%) than the value of 2.17 Å given in powder diffraction files [25]. The $2\Theta$ positions of the (1 1 0) and (2 2 0) reflections are close to the expected values [25].

The X-ray diffraction spectrum shown in Fig. 1c for a $Co_{27}Pt_{73}$ implanted sample exhibits scattering lines from $CoPt_3$ [26]. Again, the predominant orientation observed is (1 1 1), with additional weaker lines from the (1 1 0), (2 0 0) and (2 2 0) reflections. The lattice constant calculated from the (1 1 1) lattice spacing is 3.84 Å, close to the published value of 3.85 Å for the bulk intermetallic FCC $L1_2$ alloy [11]. These results are from a sample annealed at 1100°C for 2 h followed by a 120 h anneal at 700°C, the latter chosen to be below the ordering temperature for $CoPt_3$. An X-ray spectrum was also obtained after the 1100°C anneal. The two spectra are similar, with only small changes in the relative peak intensities occurring after the second anneal; hence, no significant increase in ordering occurred as a result of the low-temperature anneal.

The spectra in Fig. 1 are from samples where the implant ratios were chosen to be close to the stoichiometry of known $Co_{1-x}Pt_x$ alloys. X-ray spectra have also been obtained from additional samples implanted with $x$ in the range $36 < x < 60$. In all cases, scattering is observed from chemically ordered CoPt, as evidenced by the presence of the (1 1 0) superstructure peak. However, the lattice constants and peak intensities vary somewhat with composition. In general, as the Pt implant fraction increases over this range, the X-ray peaks shift to lower angles, indicative of increasing lattice dimensions as would be expected for incorporation of more of the larger Pt atoms in the alloy. For example, for Pt fractions of 53% and 60% the strongest X-ray scattering is from (1 1 1) planes. The (1 1 1) lattice spacing for these two samples,

calculated using corresponding $2\Theta$ positions of the (1 1 1) peak, is 2.19 and 2.21 Å, respectively, or slightly larger at the higher Pt concentration. The (1 1 1) reflection is not identified in spectra for which the Pt implant concentration is between 36% and 51%. If the lattice continues to shrink with decreasing Pt concentration, observation of (1 1 1) scattering in this range would be complicated by interference from the strong scattering yield of the $Al_2O_3$ (0 0 0 6) substrate line. In addition, as the Pt component increases from 36% to 60%, the (1 1 0) reflection shifts to smaller $2\Theta$ values consistent with an increase in lattice spacing. Both (2 2 0) and (2 0 2) reflections, that are not resolved, are also seen in these spectra, with the relative amount of scattering into the (2 0 2) peak increasing with decreasing Pt. It is interesting to note that both the $Co_{64}Pt_{36}$ and $Co_{40}Pt_{60}$ spectra contain at least some strained FCT CoPt since they both exhibit a (2 0 2) shoulder on the high angle side of the (2 2 0) peak. A (2 0 2) reflection is not expected from cubic $Co_3Pt$ or $CoPt_3$ phases. Chen et al. [2] report evidence for the $L1_0$ phase in a sample with a Pt concentration of 70%. Additional work is needed to determine the Co:Pt implant ratios where formation of the $L1_2$ phase becomes favored over the $L1_0$ phase.

Fig. 2 shows plan-view TEM micrographs from three Co–Pt alloys. Figs. 2a and c are from the same samples used for the X-ray scattering spectra in Fig. 1a and c, respectively. Fig. 2b is from a sample implanted to $Co_{55}Pt_{45}$. All three micrographs were taken under bright field conditions using the transmitted spot. It is evident that Co–Pt nanoparticles form for the processing conditions used for all three compositions. The micrograph in Fig. 2b shows particles that are strongly faceted and oriented with respect to each other and the substrate. The lateral dimensions of the largest particles seen are close to 25 nm. It should be noted that a high-resolution $\Theta - 2\Theta$ scan across the (1 1 1) reflection from a sample implanted at a slightly different Co:Pt ratio, $Co_{49}Pt_{51}$, yields a coherence length of $\sim$20 nm for the direction normal to the surface. This is consistent with the dimensions seen in Fig. 2b and suggests particles with dimensions of this order may be formed for a range of compositions near 50:50. An X-ray spectrum from the sample of Fig. 2b has a (1 1 0) superstructure peak indicating that at least some of the alloy has the $L1_0$ ordered structure. Particle dimensions of the $Co_{74}Pt_{26}$ alloy seen in the micrograph given in Fig. 2a are $<$50 nm, with the majority of particles sizes in either the range $\sim$20–30 nm or less than $\sim$10 nm. Some faceting is observed. A detailed diffraction contrast analysis was not made, and consequently, the strongly contrasting dark and light regions are tentatively attributed to the misorientation of the particles with the electron beam. In Fig. 2c the micrograph from a $Co_{27}Pt_{73}$ sample shows fairly small particles with a size distribution peaked at $\sim$9 nm and ranging up to $\sim$20 nm.

An order parameter $S$, which is a measure of the fraction of Co and Pt atoms on their ideal lattice sites, can be defined from the ratio of the integrated intensities in superstructure to fundamental X-ray peaks compared to predicted values [27]. The order parameter has been estimated from the ratio of the integrated intensities in the superstructure (1 1 0) peak to the fundamental (2 2 0) peaks in the $\Theta - 2\Theta$ spectrum in Fig. 1b compared to a theoretical calculation of the expected intensities based on atomic scattering factors, Debye–Waller factors, Lorenz polarization factors, and taking into account the thin-film geometry of the implanted CoPt layer. A value of $\sim$0.4 for the order parameter is obtained. This suggests $<$70% of the Co and Pt atoms are located on their correct $L1_0$ lattice sites. Hence, the alloy is not well-ordered in this case. (Note that the maximum order parameter for non-equiatomic compositions is less than 1. For a $Co_{47}Pt_{53}$ alloy, $S_{max}$ is 0.94.) It is interesting to note that the $S$-parameter for $Fe_{48}Pt_{52}$ nanoparticles, synthesized using similar implantation and annealing processing, shows such particles are fully ordered [17]. High $S$ values for $Fe_{55}Pt_{45}$ sputtered films and lower values for $Co_{46}Pt_{54}$ films have been previously reported [28]. From the Co–Pt binary phase diagram [24], the ordering temperature for bulk CoPt is below 825°C, whereas the Co–Pt alloy in Fig. 1b was formed by heating at 1100°C for 2 h and then cooling to room temperature in $\sim$0.5 h. Ristau et al. [29] were able to increase the order in Co–Pt films by prolonged heating at

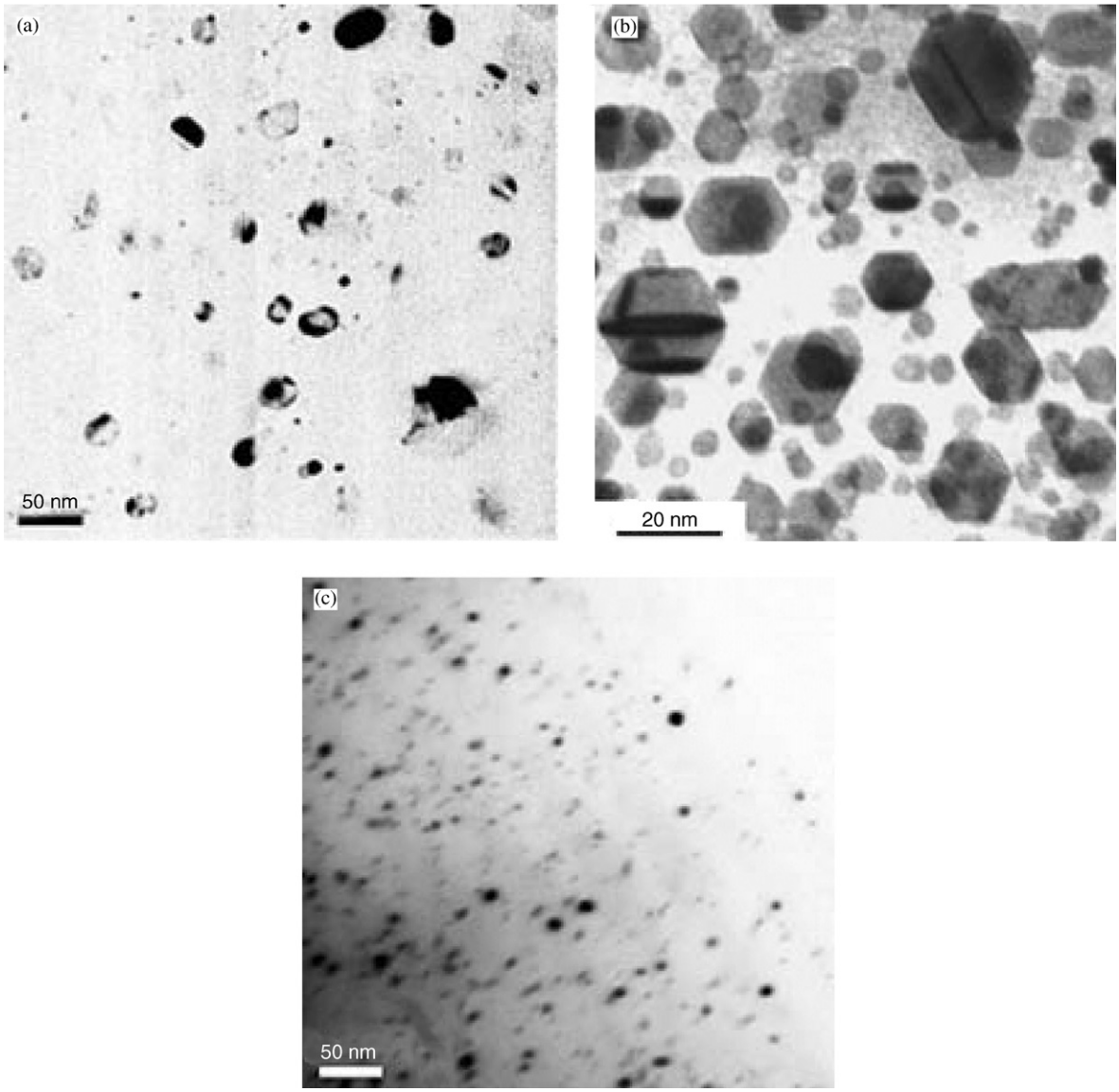


Fig. 2. Plan-view TEM micrographs from three different Co–Pt alloys. Figs. 2a and c are from the same samples as Figs. 1a and c, respectively. Fig. 2b is from a $Co_{55}Pt_{45}$ sample annealed at 1100°C for 2 h in Ar + 4% $H_2$.

temperatures below 825°C. Attempts were made using several heating schemes to increase $S$, including heating at 1100°C for 2 h followed by heating for up to an additional 140 h at 700°C or 750°C, or heating for up to 8 h at 1100°C. No value for $S$ greater than $\sim$0.44 was obtained. Annealing only at 760°C for 20 h without heating at any higher temperature led to the lowest order parameter measured, i.e., a value of $S$ less than 0.3. It should be noted that estimates for the long-range order parameter should ideally use peak intensities measured from rocking curves so as to

integrate over the entire peak. However, because of the overlap of the (2 2 0) and (2 0 2) peaks this was not possible here.

RBS spectra have been obtained from samples both as-implanted and after annealing. Typical results are given in Fig. 3a for a $Co_{54}Pt_{46}$ sample implanted at 550°C (Co) and 500°C (Pt) and in Fig. 3b for a $Co_{55}Pt_{45}$ sample implanted at 200°C (both Co and Pt). Aligned and random RBS spectra are shown following annealing at 1100°C for 2 h in Ar + 4%$H_2$. In addition, random RBS spectra are given from as-implanted samples. As marked in these figures, scattering at energies below ~1.3 MeV is from the Al and O substrate atoms. At higher energies, scattering from the implanted Co and Pt are easily resolved. The Co and Pt random yields, both as-implanted (solid line) and after thermal annealing (triangles), are essentially the same, which indicates no loss of Co or Pt during the anneal and that little long-range diffusion is occurring. For the higher-temperature implantation, significant channeling is observed in the aligned spectra after annealing (circles). Combined with the existence of CoPt lines in X-ray spectra from the same samples and the absence of pure Pt or Co reflections, these channeling results are indicative of the formation of a CoPt phase aligned with the substrate. Channeling, but to a lesser degree, is also seen in the Co and Pt yields of Fig. 3b for the 200°C implantation case. Finally, it should be mentioned that the RBS yield in the Co and Pt peaks from an as-implanted aligned spectrum (not shown) is the same as measured in the as-implanted random spectra. This demonstrates that an ordered alloy aligned with respect to the substrate only forms as a result of the heating.

Implantation for the doses and temperatures used here creates considerable damage in the substrate over the range of ion implantation, as seen in Fig. 3. Recrystallization of these damaged regions occurs at the 1100°C annealing temperature used to create the alloys, although it should be noted that recovery of the substrate can be complicated by the fact that fully amorphized α-$Al_2O_3$ first transforms quickly into a cubic γ-$Al_2O_3$ phase which then subsequently slowly transforms back into α-$Al_2O_3$ [30,31]. This transformation

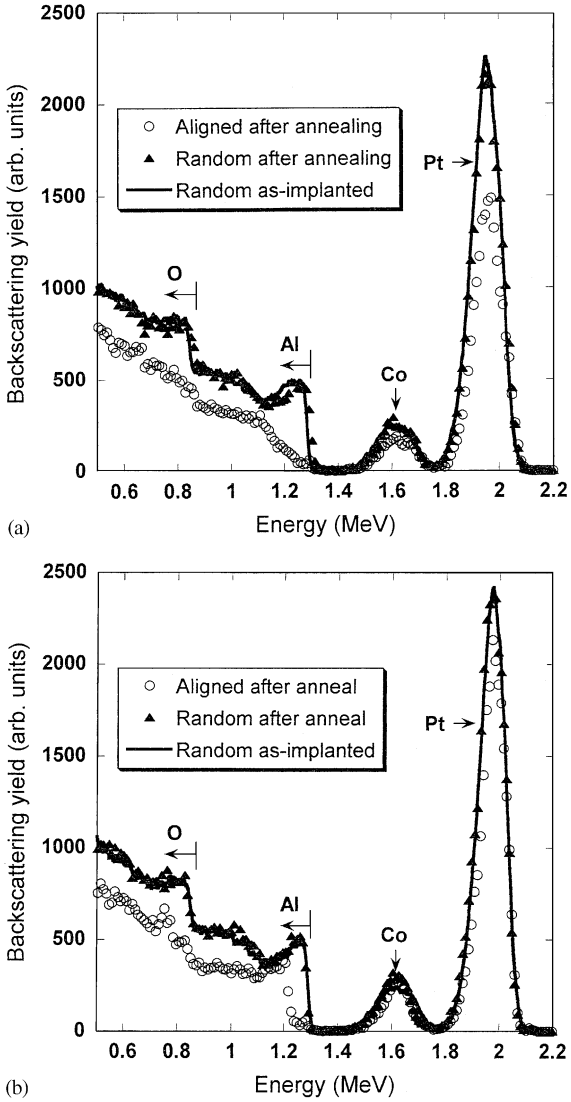


Fig. 3. Rutherford backscattering spectra from $Co_{47}Pt_{53}$ in $Al_2O_3$ for implantation at: (a) 550°C (Co) and 500°C (Pt) and (b) 200°C. Spectra obtained with the incident He beam aligned along the substrate *c*-axis (circles) and randomly oriented (triangles) are shown. Also given is a random spectrum from the as-implanted samples (solid lines).

may also affect the alloy synthesis. Most of the implants for this work were made at elevated temperatures to avoid amorphization, and RBS spectra indicate that the substrates typically were not amorphized at any depth except for a few

samples implanted at 200°C at high Pt fractions. In those cases where amorphization did occur, $\gamma$-$Al_2O_3$ reflections were detected in the corresponding X-ray data. For example, $\gamma$-$Al_2O_3$ reflections were observed in an X-ray spectrum (not given) corresponding to the 200°C-implanted sample of Fig. 3b. Interestingly, this X-ray spectrum has no peaks that can be identified with FCT CoPt, unlike the diffraction spectrum from a sample implanted at the same doses but at 550°C (Co)/500°C (Pt) which does have a CoPt(1 1 0) peak. Hence, the implant temperature makes a significant difference in the structure of the alloy formed. Over the energy range ~1.1–1.2 MeV in Fig. 3, (i.e., the part of the spectrum showing backscattering from Al in the region of highest implantation damage), the post-annealing channeling results from the substrate differ markedly for the two implantation temperatures. For the sample implanted at 200°C, the aligned yield is higher at these backscattering energies and is essentially the same as the random. This is likely due to the presence of $\gamma$-$Al_2O_3$ remaining after annealing.

Magnetic properties of the CoPt alloys formed in this study were studied using a SQUID magnetometer. In Fig. 4 are given magnetization curves for a $Co_{47}Pt_{53}$ alloy obtained from a sample of area 0.46 cm × 0.46 cm. The sample was implanted at high temperature (Co 550°C/Pt 500°C) and then annealed for 2 h at 1100°C followed by further heating for 120 h at 700°C. Curves are given for the applied field oriented both parallel and perpendicular to the substrate surface at temperatures $T = 5$ K (Fig. 4a) and 300 K (Fig. 4b). At the lower temperature, the saturation moment is $\sim 450 \times 10^{-6}$ emu, which corresponds to an average moment/atom of 1.0 $\mu_B$.

The dependence on composition for the average moment $\langle \mu \rangle$ in these nanoparticles is shown in Fig. 5. Results from this study (solid circles) trend downward as the Pt content increases. For comparison, earlier results on bulk alloys are included. Values with low Pt content, $x < 15$ at %, are taken from Crangle and Parsons [32], while values for $x > 79$ at % are from Crangle and Scott [33]. Bulk values over a wide compositional range are taken from Sanchez et al. [12] for both ordered and disordered alloys. Interestingly, the latter

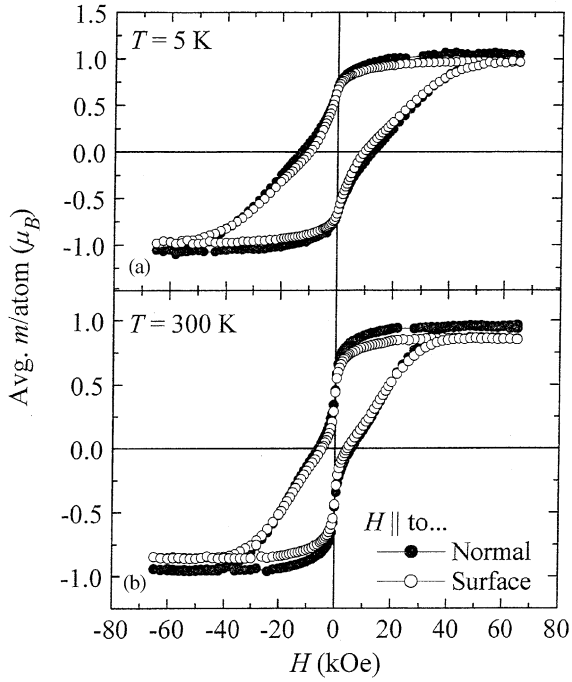


Fig. 4. Magnetization curves for a $Co_{47}Pt_{53}$ sample annealed at 1100°C for 2 h in flowing Ar + 4%$H_2$ plus a second anneal at 700°C for 120 h. Measurements were made with the sample held at: (a) 5 K and (b) 300 K, with the magnetic field applied both perpendicular and parallel to the substrate surface.

authors find that the state of order has little effect on $\langle \mu \rangle$, although ordering leads to significantly lower Curie temperatures $T_c$. This general trend differs from the magnetically and structurally similar alloys of Fe–Pt, where ordering elevates $T_c$ and depresses $\langle \mu \rangle$ [34]. Overall, the values in Fig. 5 for $\langle \mu \rangle$ of the nanoparticles lie near those of the bulk alloys and they exhibit similar compositional dependencies. The scatter for the data near the equal atom ratio ($x \sim 50$ at%) is larger than expected and may result from experimental issues related to the difficulty of saturating the high anisotropy ferromagnet or uncertainties in determining the absolute contents of Co and Pt. Alternatively, this scatter may reflect the growing importance of near-surface states for these nanoparticles. Further systematic studies will be required, however, to support or disprove this speculation.

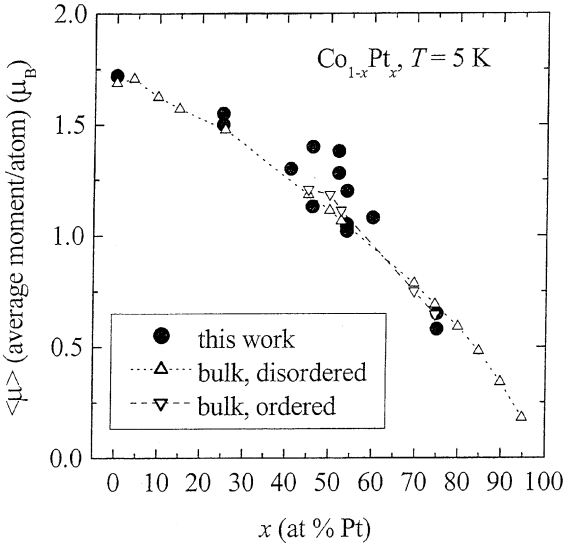


Fig. 5. The average magnetic moment per atom $\langle \mu \rangle$ versus Pt content $x$ for Co–Pt nanoparticles (filled circles). Measurements were conducted at 5 K. Open symbols show average moments for disordered and ordered bulk alloys, as described in the text. The estimated uncertainty in the moment per atom is 5–10%, due primarily to issues in removal of the substrate background signal and to uncertainty in the mass of the Co–Pt particles.

From magnetization loops like those in Fig. 4, one may obtain the coercive field $H_c$. At 5 K, the coercive field for a $Co_{47}Pt_{53}$ alloy obtained with $H$ parallel to the surface is $H_c = 9.7$ kOe. This is somewhat less than the 12.9 kOe value found at the same implant ratio with $H$ normal to the surface (see Fig. 4a). An even higher value of 14.2 kOe at 5 K was observed with $H$ normal to the surface for a $Co_{55}Pt_{45}$ sample. These values are lower limits since the magnetization may not be saturated at the maximum applied field. At $T = 300$ K in Fig. 4b, the loops have visibly narrowed, but the coercivity remains high. Similar high $H_c$ values have been reported in the literature, including 10 kOe for CoPt films [28]. There has been some discussion as to the source of the high coercivity for CoPt and the relation between order and $H_c$ (see for example, Refs. [3,28,29,35]). It has been reported that the maximum coercivity corresponds to the fully ordered alloy [29]. This suggests that if the alloys prepared here had better order, then $H_c$ could be even higher and that identifying processing conditions that controllably alter the order could be useful as a means to tailor $H_c$. The magnetization curves are not square, but show rather well-developed double shoulders including a pronounced shoulder near $H = 0$. Similar results have been reported previously, (see Refs. [8,17] and references therein). The origin of this feature, which probably indicates the presence of multiple phases, remains to be clarified.

The coercive field varies significantly with the implanted Co:Pt ratio. In Fig. 6, $H_c$ is plotted as a function of Pt concentration for the applied magnetic field parallel to the sample surface. Coercive field measurements are given at both 5 and 300 K. X-ray diffraction indicates the presence of the $L1_0$ CoPt phase over the range of Pt graphed. The maximum coercivity in the figure, $H_c = 9.7$ kOe, is obtained for a slightly Pt-rich concentration although additional data around the equiatomic Co:Pt ratio are needed to determine more precisely at what ratio the coercivity maximizes. $H_c$ falls to near-zero for Pt concentrations of 40% and 60%. A Pt concentration dependence was observed for $H_c$ for CoPt [2]

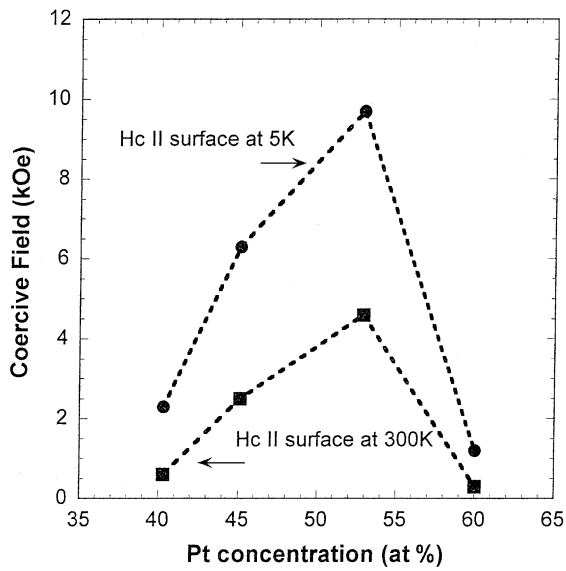


Fig. 6. Dependence of the coercive field $H_c$ on the Pt atomic fraction, measured with the applied field parallel to the sample surface.

and FePt [18,36] alloys. For the sample with the highest value in this figure, $H_c$ remained at 3.6 kOe even at 400 K.

For the Co-rich stoichiometric alloy $Co_3Pt$, the coercivity is rather low, approximately 1000 Oe at 5 K and 250 Oe at 300 K. We note that Harp et al. [9] discovered an HCP-structured $Co_3Pt$ phase with high magnetic anisotropy. It appears, however, that that phase likely becomes unstable above $\sim$400°C, as the uniaxial anisotropy $K_u$ collapses rapidly above this temperature [37]. Thus, we might expect low values of $H_c$, as observed, for material prepared during a high temperature anneal at 1100°C used in the present work.

## 4. Conclusions

$Co_{1-x}Pt_x$ alloy nanoparticles have been synthesized by co-implanting Co and Pt into bulk in $Al_2O_3$ followed by thermal annealing. The stoichiometric phases that form depend on the implant ratio of the two species. For implants of $Co_{1-x}Pt_x$ where $0.36<x<0.6$, at least partial ordering into the $L1_0$ CoPt microstructure is observed. Likewise, for $x$ close to 0.25 or 0.75, phases of $Co_3Pt$ and $CoPt_3$, respectively, are present. These alloys are oriented with the matrix but exhibit multiple distinct orientations. The CoPt nanoparticles do not approach a well-ordered $L1_0$ structure, even after extensive anneals at temperatures below the ordering temperature. The CoPt is ferromagnetic with coercivities as high as 14.2 kOe for the applied field normal to the surface. For a $Co_{47}Pt_{53}$ alloy, the coercive field measured for $H$ parallel to the surface shows a significant dependence on the Co:Pt ratio. Significant magnetic hysteresis persists to at least 400 K. The synthesized alloys do not exhibit simple magnetization curves.

Recently, CoPt nanoparticles have also been formed in fused $SiO_2$ using ion implantation and annealing [38]. The particles are randomly oriented and are ferromagnetic, with a coercive field as high as 9 kOe at 5 K. These data will be presented separately.

## Acknowledgements

The authors are indebted to D.K. Thomas and D.K. Hensley for help with implantation of the samples. Part of this research was sponsored by the Laboratory Directed Research and Development Program of Oak Ridge National Laboratory. Oak Ridge National Laboratory is managed by UT-Battelle, LLC, for the US Department of Energy under Contract DE-AC05-00OR22725.

## References

[1] S. Jeong, Y.-N. Hsu, M.E. McHenry, D.E. Laughlin, J. Appl. Phys. 87 (2000) 6950.
[2] C. Chen, O. Kitakami, S. Okamoto, Y. Shimada, J. Appl. Phys. 87 (2000) 6947.
[3] A. Kumbhar, L. Spinu, F. Agnoli, K.-Y. Wang, W. Zhou, C.J. O'Connor, IEEE Trans. Magn. 37 (2001) 2216.
[4] K. Barmak, R.A. Ristau, J. Appl. Phys. 79 (1996) 5330.
[5] M. Yu, Y. Liu, D.J. Sellmyer, J. Appl. Phys. 87 (2000) 6959.
[6] R.A. McCurrie, P. Gaunt, Philos. Mag. 13 (1966) 567.
[7] T. Devolder, H. Bernas, D. Ravelosona, C. Chappert, S. Pizzini, J. Vogel, J. Ferre, J.-P. Jamet, Y. Chen, V. Mathet, Nucl. Instrum. Methods B 175–177 (2001) 375.
[8] S.-E. Park, P.-Y. Jung, K.-B. Kim, J. Appl. Phys. 77 (1995) 2641.
[9] G.R. Harp, D. Weller, T.A. Rabedeau, R.F.C. Farrow, M.F. Toney, Phys. Rev. Lett. 71 (1993) 2493.
[10] S. Ferrer, P. Fajardo, F. de Bergevin, J. Alvarez, X. Torrelles, H.A. van der Vegt, V.H. Etgens, Phys. Rev. Lett. 77 (1996) 747.
[11] M. Li, Z.-H. Jiang, Z.-Q. Zou, D.-F. Shen, J. Magn. Magn. Mater. 176 (1997) 331.
[12] J.M. Sanchez, J.L. Moran-Lopez, C. Leroux, M.C. Cadeville, J. Phys: Condens. Matter 1 (1989) 491.
[13] R.S. Bandhu, R. Sooryakumar, R.F.C. Farrow, D. Weller, M.F. Toney, T.A. Rabedeau, J. Appl. Phys. 91 (2002) 2737.
[14] Y. Yamada, W.P. Van Drent, E.N. Abarra, T. Suzuki, J. Appl. Phys. 83 (1998) 6527.
[15] A. Kashyap, K.B. Garg, A.K. Solanki, T. Nautiyal, S. Auluck, Phys. Rev. B 60 (1999) 2262.
[16] C.-J. Lin, G.L. Gorman, Appl. Phys. Lett. 61 (1992) 1600.
[17] C.W. White, S.P. Withrow, J.D. Budai, L.A. Boatner, K.D. Sorge, J.R. Thompson, K.S. Beaty, A. Meldrum, Nucl. Instrum. Methods B 191 (2002) 437.
[18] C.W. White, S.P. Withrow, J.D. Budai, L.A. Boatner, K.D. Sorge, J.R. Thompson, K.S. Beaty, A. Meldrum, Mater. Res. Soc. Symp. Proc. 704 (2002) 187.
[19] A. Meldrum, R.F. Haglund, L.A. Boatner, C.W. White, Adv. Mater. 13 (2001) 1431.

[20] T. Devolder, Phys. Rev. B 62 (2000) 5794.
[21] K.S. Beaty, A. Meldrum, J.P. Franck, K. Sorge, J.R. Thompson, C.W. White, R.A. Zuhr, S. Honda, Mater. Res. Soc. Symp. Proc. 703 (2002) 331.
[22] S. Honda, F.A. Modine, T.E. Haynes, A. Meldrum, J.D. Budai, K.J. Song, J.R. Thompson, L.A. Boatner, Mater. Res. Soc. Symp. Proc. 581 (2000) 71.
[23] J.F. Ziegler, J.P. Biersack, U. Littmark, The Stopping and Range of Ions in Solids, Pergamon Press, New York, 1985.
[24] T.B. Massalski (Editor-in-chief), Phase Diagrams: Binary Alloy Phase Diagrams, Vol. 1, American Society for Metals, Metals Park, OH, 1986, p. 791.
[25] JCPDS-International Centre for Diffraction Data, Powder Diffraction File #43-1358, ICDD, Newtown Square, PA, 1997.
[26] JCPDS-International Centre for Diffraction Data, Powder Diffraction File #29-0499 ICDD, Newtown Square, PA, 1997.
[27] B.E. Warren, X-ray Diffraction, Addison-Wesley, Reading, MA, 1969, p. 206.
[28] S. Jeong, Y.-H. Hsu, D.E. Laughlin, M.E. McHenry, IEEE Trans. Magn. 37 (2001) 1299.
[29] R.A. Ristau, K. Barmak, L.H. Lewis, K.R. Coffey, J.K. Howard, J. Appl. Phys. 86 (1999) 4527.
[30] C.W. White, C.J. McHargue, P.S. Sklad, L.A. Boatner, G.C. Farlow, Mater. Sci. Rep. 4 (1989) 41.
[31] P.S. Sklad, J.C. McCallum, C.J. McHargue, C.W. White, Nucl. Instrum. Methods B 46 (1990) 102.
[32] J. Crangle, D. Parsons, Proc. Roy. Soc. A 253 (1960) 509.
[33] J. Crangle, W.R. Scott, J. Appl. Phys. 36 (1965) 921.
[34] Landolt-Bornstein New Series III, Magnetic Properties of Metals, Vol. 19a, Springer, Heidelberg, 1988.
[35] Y. Tanaka, N. Kimura, K. Hono, K. Yasuda, T. Sakurai, J. Magn. Magn. Mater. 170 (1997) 289.
[36] S. Sun, C.B. Murray, D. Weller, L. Folks, A. Moser, Science 287 (2000) 1989;
S. Sun, C.B. Murray, D. Weller, L. Folks, A. Moser, IEEE Trans. Magn. 37 (2001) 1239.
[37] D. Weller, A. Moser, L. Folks, M.E. Best, L. Wen, M.F. Toney, M. Schwickert, J.-U. Thiele, M.F. Doerner, IEEE Trans. Magn. 36 (2000) 10.
[38] S.P. Withrow, unpublished data.